

Optically induced electron spin currents in the Kretschmann configuration

Daigo Oue^{1,2} and Mamoru Matsuo^{1,3}

¹*Kavli Institute for Theoretical Sciences, University of Chinese Academy of Sciences, Beijing, 100190, China.*

²*The Blackett Laboratory, Department of Physics, Imperial College London,
Prince Consort Road, Kensington, London SW7 2AZ, United Kingdom*

³*CAS Center for Excellence in Topological Quantum Computation,
University of Chinese Academy of Sciences, Beijing 100190, China*

(Dated: April 12, 2022)

We investigate electron spin currents induced optically via plasmonic modes in the Kretschmann configuration. By utilising the scattering matrix formalism, we take the plasmonic mode coupled to external laser drive into consideration and calculate induced magnetisation in the metal. The spatial distribution of the plasmonic mode is inherited by the induced magnetisation, which acts as inhomogeneous effective magnetic field and causes the Stern-Gerlach effect to drive electron spin currents in the metal. We solve spin diffusion equation with a source term to analyse the spin current as a function of the spin diffusion length of the metal, the frequency and the incident angle of the external drive.

I. INTRODUCTION

Electron spin is one of the fundamental physical quantities, which can carry heat, angular momentum, and even quantum information^{1–6}, and thus it is crucial to control the electron spin by other excitations. It has been reported that circulation or non-zero vorticity of electric charge flow induce spin current in the metal^{7–9}. In these studies, they excited inhomogeneous effective magnetic field by the circulation or the vorticity to bring about the Stern-Gerlach-type effect and drive the electron spin transport. Keeping this idea in mind, we consider optically driving electron spin current via plasmonic modes in the Kretschmann configuration.

Recently, the spin current generation from light via plasmonic modes have been studied^{10–13}. In Refs.^{10,11}, they investigated spin current generation in magneto-plasmonic systems at localised plasmon resonance conditions, where the difference of the nonequilibrium distribution functions between magnons and plasmons is utilised as in the spin pumping and the spin Seebeck effect^{14,15}. In our previous works^{12,13}, we proposed the angular momentum conversion from the transverse spin of propagating surface plasmons (SPs) to electronic systems, where the transverse spin circulates electron gas to induce inhomogeneous magnetic field and result in electron spin current in the metallic media.

However, to the best of our knowledge, it has never theoretically investigated that the electron spin dynamics in a plasmonic system where the plasmonic modes are coupled to external laser drive. In this study, we calculate the electron spin current induced optically in a trilayer system.

We consider a metal film sandwiched by two different dielectrics (FIG. 1). Let the permittivity of the metal ϵ_m and those of dielectrics ϵ_a and ϵ_p ($\epsilon_a < \epsilon_p$). This layered system is called the Kretschmann configuration which is one of the typical systems to excite plasmonic modes by a laser drive¹⁶. When the laser is incident on the metal film from one dielectric side where the permittivity

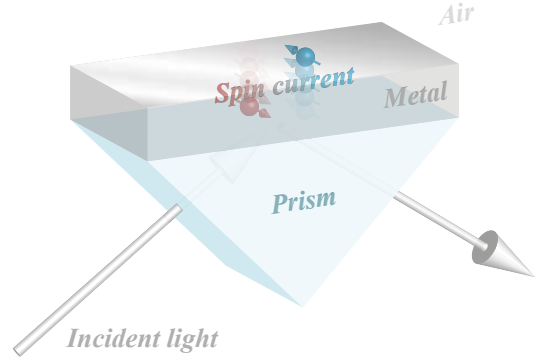


FIG. 1. Optically driven electron spin current in a trilayer system (Kretschmann configuration), where a metal film ($\epsilon = \epsilon_m$) with a thickness of d is sandwiched by two dielectrics, air ($\epsilon_a = 1$) and prism ($\epsilon_p = 1.5^2$). A laser drive field is incident on the metal from the prism side, and surface plasmon modes can be excited on the air-metal interface when the incident angle exceeds the critical angle ($\theta_{in} > \theta_c \equiv \arcsin \sqrt{\epsilon_a/\epsilon_p}$). In the excited plasmonic modes, the electric field is circulating, which induces orbiting motion of electron gas in the metal and results in inhomogeneous magnetisation. The electron spin experiences the Stern-Gerlach effect under the magnetisation, and the electron spin current is driven in the direction perpendicular to the air-metal interface.

is higher than the other dielectric side, surface plasmon modes can be excited above the critical angle condition ($\theta_{in} > \theta_c \equiv \arcsin(\sqrt{\epsilon_a/\epsilon_p})$).

The excited plasmonic modes have exponential profile and thus transversally spinning electric field in the metal due to the spin-momentum locking effect of light in non-paraxial regime^{17–23}. When the frequency of the field is smaller than the plasma frequency of the metal, the highly confined spinning field induces the electron gas to circulate, which generates the steep gradient of magnetisation. Although the magnetisation itself is so small

that it is even difficult to detect as analysed in the previous studies^{24,25}, its gradient can be large enough to drive electron spin transport^{12,13}.

II. MAGNETISATION INDUCED BY PLASMONIC FIELDS

To investigate the electron dynamics in the plasmonic field, we firstly calculate the electromagnetic field by a scattering matrix formalism, and evaluate magnetisation induced by the field in the metal. Once we obtain the frequency dependence, the incident angle dependence, and the spatial distribution of the magnetisation, the diffusive dynamics of electron spin can be calculated from spin diffusion equation with a source term^{26,27}.

A. Scattering matrix formalism for a multilayer system

Our trilayer system has translational invariance in x and y direction, and it is convenient to use wavenumber, k_x and k_y , as parameters in the Maxwell equations rather than x and y . Also, we work in the frequency domain (i.e., use ω rather than t) to have a wave equation,

$$\left[-\frac{\partial^2}{\partial z^2} - \left(\frac{\omega^2}{c^2} \epsilon - k_{\parallel}^2 \right) \right] \mathbf{E}(\mathbf{k}_{\parallel}, \omega) = 0. \quad (1)$$

Here, we have used

$$\mathbf{k}_{\parallel} = \begin{pmatrix} k_x \\ k_y \end{pmatrix}, \quad k_{\parallel} = \sqrt{k_x^2 + k_y^2}.$$

We solve Eq. (1) in each layer to get the electric field, and substitute it into

$$\mathbf{H}(\mathbf{k}_{\parallel}, \omega) = \frac{1}{\omega \mu_0} \begin{pmatrix} k_x \\ k_y \\ -i \frac{\partial}{\partial z} \end{pmatrix} \times \mathbf{E}(\mathbf{k}_{\parallel}, \omega) \quad (2)$$

to calculate the magnetic field. Here, μ_0 is the permeability of vacuum.

The electromagnetic field should satisfy the boundary conditions of the Maxwell equations,

$$\begin{pmatrix} k_x \\ k_y \\ -i \frac{\partial}{\partial z} \end{pmatrix} \cdot \mathbf{E}(\mathbf{k}_{\parallel}, \omega) = 0, \quad \begin{pmatrix} k_x \\ k_y \\ -i \frac{\partial}{\partial z} \end{pmatrix} \cdot \mathbf{H}(\mathbf{k}_{\parallel}, \omega) = 0. \quad (3)$$

Under these conditions, two kinds of polarisation are possible solution of the vector wave equation (1). We define those two polarisation vectors,

$$e_{\lambda\sigma} = \begin{cases} \frac{\mathbf{k}_{\sigma} \times \mathbf{k}_{\sigma} \times \mathbf{u}_z}{|\mathbf{k}_{\sigma} \times \mathbf{k}_{\sigma} \times \mathbf{u}_z|} & \lambda = p, \\ \frac{\mathbf{k}_{\sigma} \times \mathbf{u}_z}{|\mathbf{k}_{\sigma} \times \mathbf{u}_z|} & \lambda = s, \end{cases} \quad (4)$$

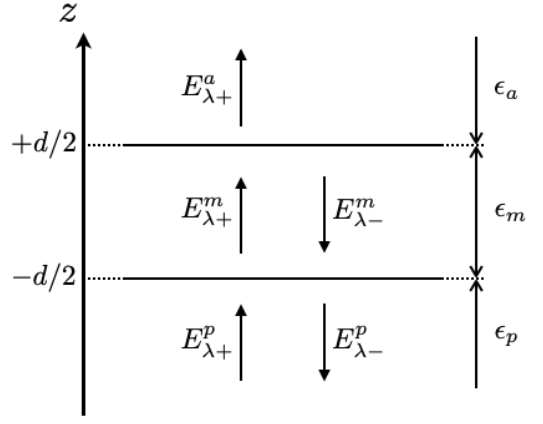


FIG. 2. Electromagnetic field in each layer is expanded by the eigenmodes as in (6) and (7). We set the amplitudes of the fields with a polarisation of $\lambda = s, p$ in the prism, metal, and air layers $E_{\lambda\sigma}^{p,m,a}$, respectively, where $\sigma = \pm$ specifies the direction of the z components of the wavevectors. The permittivity in each layer is $\epsilon_{a,m,p}$. The frequency ω and the wavenumber in the direction parallel to the interfaces \mathbf{k}_{\parallel} ($|\mathbf{k}_{\parallel}|^2 < \omega^2 \epsilon_p / c^2$) are free parameters. We impose the field continuity (boundary conditions) at $z = \pm d/2$ in order to derive simultaneous equations determining the scattering matrix of this trilayer system (9).

where

$$\mathbf{k}_{\sigma}(k_{\parallel}, \omega) = \begin{pmatrix} \mathbf{k}_{\parallel} \\ \sigma K(k_{\parallel}, \omega) \end{pmatrix}, \quad K(k_{\parallel}, \omega) = \sqrt{\frac{\omega^2}{c^2} \epsilon - k_{\parallel}^2}. \quad (5)$$

Here, $K(k_{\parallel}, \omega)$ is the wavenumber in the z direction, and $\sigma = \pm$ specifies the propagation direction (i.e., $\sigma = \pm$ means that the wave propagates in the $\pm z$ direction).

In terms of the polarisation vectors, the electric and magnetic field in each layer can be written as

$$\mathbf{E}(\mathbf{k}_{\parallel}, \omega) = \sum_{\lambda\sigma} e_{\lambda\sigma}^l e^{i\sigma K_l z} E_{\lambda\sigma}^l, \quad (6)$$

$$\mathbf{H}(\mathbf{k}_{\parallel}, \omega) = \frac{1}{Z_0} \sum_{\lambda\sigma} \sqrt{\epsilon_l} e_{\lambda\sigma}^l e^{i\sigma K_l z} E_{\lambda\sigma}^l, \quad (7)$$

where $Z_0 = \sqrt{\mu_0 / \epsilon_0}$ is the impedance of free space, and ϵ_0 is the permittivity of vacuum. Also, $l = a, m, p$ specifies a medium in which the field lives, air, metal or prism layers, and $E_{\lambda\sigma}^l$ is the modal amplitude of the field with given polarisation and propagation direction in each layer. Note that we here have defined $\bar{p} = s$ and $\bar{s} = p$.

Let us take the coordinate so that the wavevector lies in the xz plane ($k_x = k, k_y = 0$), and fix $\lambda = p$. This is because we are interested in plasmonic excitations, and there is no SPs excited by the s polarisation. Then, we have

$$e_{p\sigma}^l = \frac{c/\sqrt{\epsilon_l}}{\omega} \begin{pmatrix} \sigma K_l \\ 0 \\ -k \end{pmatrix}, \quad e_{s\sigma}^l = \begin{pmatrix} 0 \\ -1 \\ 0 \end{pmatrix}. \quad (8)$$

Now, we are ready to derive the scattering matrix of our system. Imposing the continuities of the tangential fields, E_z and H_y , at the two interfaces ($z = \pm d/2$), we can obtain simultaneous equations in the matrix form,

$$S^{-1}\psi_{\text{out}} = \psi_{\text{in}} \quad (9)$$

$$S^{-1} = \begin{pmatrix} -\frac{K_a}{\sqrt{\epsilon_a}}e^{+iK_a d/2} & \frac{K_m}{\sqrt{\epsilon_m}}e^{+iK_m d/2} & -\frac{K_m}{\sqrt{\epsilon_m}}e^{-iK_m d/2} & 0 \\ -\sqrt{\epsilon_a}e^{+iK_a d/2} & \sqrt{\epsilon_m}e^{+iK_m d/2} & \sqrt{\epsilon_m}e^{-iK_m d/2} & 0 \\ 0 & \frac{K_m}{\sqrt{\epsilon_m}}e^{-iK_m d/2} & -\frac{K_m}{\sqrt{\epsilon_m}}e^{+iK_m d/2} & \frac{K_p}{\sqrt{\epsilon_p}}e^{+iK_p d/2} \\ 0 & \sqrt{\epsilon_m}e^{-iK_m d/2} & \sqrt{\epsilon_m}e^{+iK_m d/2} & -\sqrt{\epsilon_p}e^{+iK_p d/2} \end{pmatrix}, \quad (10)$$

and output and input vectors,

$$\psi_{\text{out}} = \begin{pmatrix} E_{p+}^a \\ E_{p+}^m \\ E_{p-}^m \\ E_{p-}^p \end{pmatrix}, \quad \psi_{\text{in}} = \begin{pmatrix} 0 \\ 0 \\ \frac{K_p}{\sqrt{\epsilon_p}}e^{-iK_p d/2} \\ \sqrt{\epsilon_p}e^{-iK_p d/2} \end{pmatrix} E_{p+}^p. \quad (11)$$

The 2×2 block matrices in the diagonal entries of S^{-1} contain the information of plasmonic modes. Indeed, the determinant of the left top block matrix returns the standard dispersion relation of the SP mode at the air-metal interface¹⁶,

$$\det \begin{pmatrix} -\frac{K_a}{\sqrt{\epsilon_a}}e^{+iK_a d/2} & \frac{K_m}{\sqrt{\epsilon_m}}e^{+iK_m d/2} \\ -\sqrt{\epsilon_a}e^{+iK_a d/2} & \sqrt{\epsilon_m}e^{+iK_m d/2} \end{pmatrix} = 0, \quad \frac{K_m/\epsilon_m}{K_a/\epsilon_a} = -1, \quad (12)$$

whereas that of the right bottom block matrix returns the dispersion of the SP mode at the metal-prism,

$$\det \begin{pmatrix} -\frac{K_m}{\sqrt{\epsilon_m}}e^{+iK_m d/2} & \frac{K_p}{\sqrt{\epsilon_p}}e^{+iK_p d/2} \\ -\sqrt{\epsilon_m}e^{+iK_m d/2} & \sqrt{\epsilon_p}e^{+iK_p d/2} \end{pmatrix} = 0, \quad \frac{K_m/\epsilon_m}{K_p/\epsilon_p} = -1.$$

From (9), we can derive the amplitudes of the electric and magnetic fields in the system excited by the given input (see FIG. 3). Here, we use the Drude free electron model for the permittivity of the metal,

$$\epsilon_m = 1 - \frac{\omega_p^2}{\omega^2}. \quad (13)$$

where the scattering matrix of our system is defined by

We can define the incident angle such that

$$k = \frac{\omega}{c}\sqrt{\epsilon_p}\sin\theta_{\text{in}}, \quad K_p = \frac{\omega}{c}\sqrt{\epsilon_p}\cos\theta_{\text{in}}. \quad (14)$$

In other words, the incident angle is given by

$$\theta_{\text{in}} = \arctan\left(\frac{k}{K_p}\right). \quad (15)$$

When the incident angle is below the critical angle ($\theta_{\text{in}} < \theta_c \equiv \arcsin\sqrt{\epsilon_a/\epsilon_p}$), the incident field is transmitted into the other side as in the FIG. 3a. In this case, there is no excited SP mode. On the other hand, if the incident angle exceeds the critical angle, then the SP mode can be excited under wavenumber matching condition,

$$\frac{\omega}{c}\sqrt{\epsilon_p}\sin\theta_{\text{in}} = k_{\text{sp}}(\omega), \quad \theta_{\text{in}} = \arcsin\left[\frac{k_{\text{sp}}(\omega)}{\omega\sqrt{\epsilon_p}/c}\right] \equiv \theta_{\text{sp}}, \quad (16)$$

where $k_{\text{sp}}(\omega)$ can be determined by solving the dispersion relation (12) for the wavenumber k . In FIG. 3c, the SP mode excitation at the wavenumber matching condition (16) is shown. While the field in the air layer has uniform spatial distribution in the critical incidence case ($\theta_{\text{in}} = \theta_c$) shown in FIG. 3b, the field is compressed at the air-metal interface at the wavenumber matching condition.

B. Inhomogeneous induced magnetisation

With the modal amplitudes calculated by the scattering matrix method in the previous part II A, we can derive the angular momentum (AM) density of electron gas

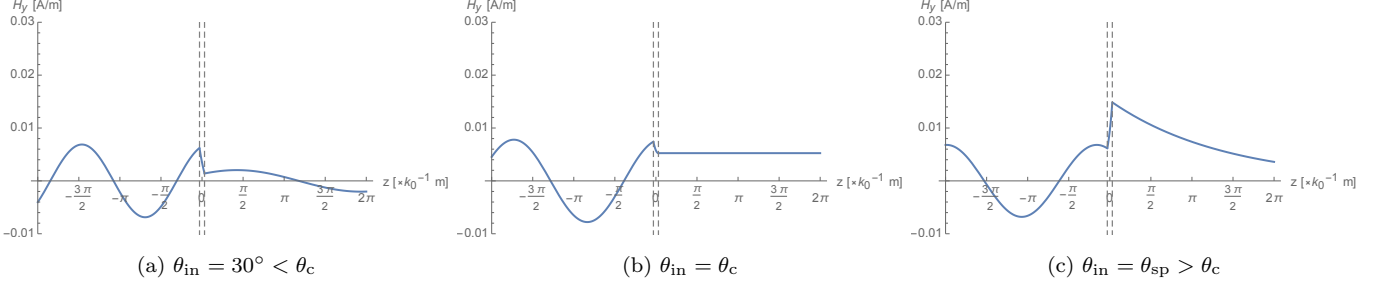


FIG. 3. The field distribution in the trilayer system. The metal region ($-d/2 \leq z \leq d/2$) is indicated by the dashed grey lines. (a) The incident angle is smaller than the critical angle between the prism and the air layers ($\theta_{\text{in}} < \theta_c \equiv \arcsin \sqrt{\epsilon_a/\epsilon_p}$). We can confirm that the incident field is decay in the metal layer and transmitted into the other side. (b) The critical angle incidence $\theta_{\text{in}} = \theta_c$. At the critical angle, the electromagnetic field in the air layer is single plane wave, and the magnetic field distribution is uniform in the z direction. (c) The incident angle is SP angle θ_{sp} at which the x component of the incident wavevector is matched with that of the SP. It is clear that the SP is excited at the interface between metal and air layers. The electromagnetic energy of the SP is compressed at the interface, and the field has exponential profile in the air region unlike the plane wave at the critical angle. In order to generate these plots, we set the incident frequency $\omega = ck_0 = 2.88 \times 10^{15}$ Hz ($k_0 = 2\pi/655 \text{ nm}^{-1}$), the incident amplitude $E_{p+}^p = 1.0$ V/m, and $\omega_p = 2\pi \times 2.1 \times 10^{15}$ Hz (the plasma frequency of gold).

in the metal in terms of the electric field^{12,13,25},

$$\mathbf{S}_{el} = \frac{1}{4} \epsilon_0 \frac{d\epsilon}{d\omega} \Im \mathbf{m} (\mathbf{E}^* \times \mathbf{E}) \quad (17)$$

$$= \frac{1}{2} \frac{k \Im \mathbf{m} (K_m)}{\omega^2 \epsilon_m / c^2} \frac{d\epsilon_m}{d\omega} \epsilon_0 \sum_{\sigma} \sigma |E_{p\sigma}^m|^2 e^{-2\sigma \Im \mathbf{m} (K_m) z} \mathbf{u}_y \quad (18)$$

$(-d/2 \leq z \leq +d/2).$

By simply multiplying the AM of the electron gas by the gyromagnetic ratio $\gamma = \frac{e}{2m}$, we can evaluate the magnetisation induced by the angular motion of the electron gas,

$$\mathbf{M} = \frac{1}{2} \gamma \frac{k \Im \mathbf{m} (K_m)}{\omega^2 \epsilon_m / c^2} \frac{d\epsilon_m}{d\omega} \epsilon_0 \sum_{\sigma} \sigma |E_{p\sigma}^m|^2 e^{-2\sigma \Im \mathbf{m} (K_m) z} \mathbf{u}_y. \quad (19)$$

In FIG. 4, the induced magnetisation as a function of the incident field parameters, ω and k . Since the incident angle should be smaller than 90° , the wavenumber in the x direction is limited as

$$k \leq \frac{\omega}{c} \sqrt{\epsilon_p}. \quad (20)$$

Also, note that any excitations cannot go beyond the light line ($\omega \leq ck$). Therefore, the induced magnetisation which can be excited in the Kretschmann configuration is only between the two diagonal dashed lines in FIG. 4. There is a peak in the region, which is contribution from the surface plasmon mode at the air-metal interface. If we replot the induced magnetisation as a function of the incident angle for a given incident frequency (FIG. 5), we can clearly see that there is a peak at the SP angle for a frequency of $\omega = 2\pi c / (655 \times 10^{-9}) = 2.88 \times 10^{15}$ Hz,

$$\theta_{\text{sp}} = \arcsin \sqrt{\frac{\epsilon_m}{\epsilon_a + \epsilon_m}} \approx 43^\circ.$$

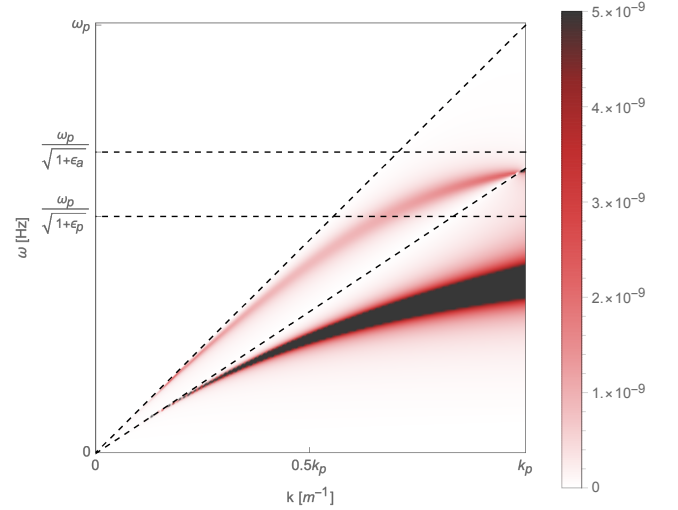


FIG. 4. Magnetisation at the metal surface $z = +d/2$ induced by the plasmonic modes as a function of the wavenumber in the x direction and the frequency of the incident field. We can see two peaks in this colormap. This is because there are two types of plasmonic excitations in our system. One is the SP at the air-metal interface which mainly contributes to the upper peak. The other is the SP at the metal-prism interface, contributing to the lower peak. The light dispersion in the air and prism, $\omega = ck/\sqrt{\epsilon_a}$ and $\omega = ck/\sqrt{\epsilon_p}$, and the surface plasma frequencies at the two interfaces, $\omega_p/\sqrt{1+\epsilon_a}$ and $\omega_p/\sqrt{1+\epsilon_p}$, are indicated by dashed lines. In this figure, we set $E_{p+}^p = \sqrt{Z_0 \times 100 \text{ mW/cm}^2} \approx 0.62 \times 10^3$ and $\omega_p = 2\pi \times 2.1 \times 10^{15}$ Hz (the plasma frequency of gold), and we defined $k_p \equiv \omega_p/c$. Note that we set the upper bound of this plot range at $0.5 \mu\text{A/m}$ because the peaks are so large that other data become invisible if we plot the full range.

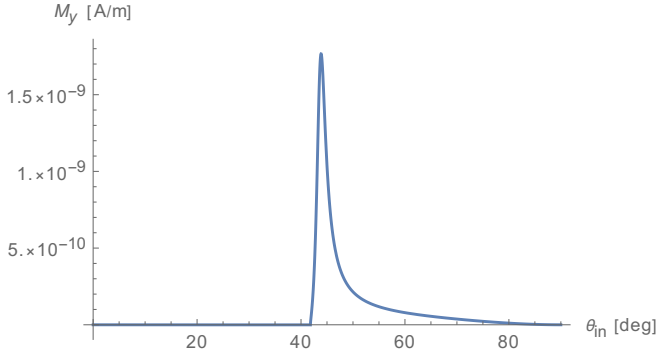


FIG. 5. Induced magnetisation at the metal surface $z = +d/2$ as a function of the incident angle. It is clear that it peaks at the SP angle incidence ($\theta_{\text{in}} = \theta_{\text{SP}} \approx 43^\circ$). We set the incident frequency $\omega = ck_0 = 2.88 \times 10^{15}$ Hz ($k_0 = 2\pi/655 \text{ nm}^{-1}$), and all other parameters are the same as the previous figures.

III. DIFFUSIVE ELECTRON SPIN DYNAMICS IN THE METAL

In this section, we analyse the electron spin dynamics in the inhomogeneous magnetic field by using the spin diffusion equation. As discussed in the literature^{26,27}, we need a source term in the diffusion equation to take two kinds of processes, spontaneous diffusion and induced diffusion, into consideration,

$$\left(\frac{\partial}{\partial t} - D_s \nabla^2 + \frac{1}{\tau} \right) \delta\mu = \rho_0 e D_s \nabla \cdot \mathbf{j}_s^{\text{sou}}, \quad (21)$$

where our source term is given by the gradient of the inhomogeneous magnetisation,

$$\mathbf{j}_s^{\text{sou}} = \frac{\hbar\mu_0}{m\rho_0} \nabla M_y. \quad (22)$$

Here, $D_s = \lambda_s^2/\tau$ is the diffusion constant, λ_s and τ are the spin diffusion length and the spin relaxation time in the metal, and ρ_0 is the resistivity of the metal. Spin accumulation $\delta\mu$ is a potential for the electron spin, and its gradient drives electron spin currents, $\mathbf{j}_s \propto \nabla\delta\mu$.

At the steady state ($\partial/\partial t = 0$), we obtain the space evolution equation of the spin accumulation,

$$\nabla^2 \delta\mu = \frac{1}{\lambda_s^2} \delta\mu + \frac{\hbar e}{m} \mu_0 \nabla^2 M_y. \quad (23)$$

There are two characteristic lengths in this equation. One is the spin diffusion length λ_s , which characterises the spontaneous diffusion process. The other is the penetration length of the plasmonic mode $\Im\mathbf{m}(K_m)$, which is hidden in the gradient operator in front of the magnetisation M_y , and characterises the diffusion process induced optically.

The particular solution of this inhomogeneous differ-

ential equation is

$$\delta\mu^{\text{SP}} = \sum_{\sigma} A_{\sigma} e^{-2\sigma\Im\mathbf{m}(K_m)z}, \quad (24)$$

$$A_{\sigma} = \sigma \frac{2k\Im\mathbf{m}(K_m)}{\omega^2 \epsilon_m / c^2} L(k, \omega, \lambda_s) \gamma \mu_B \mu_0 \frac{d\epsilon_m}{d\omega} u_{\sigma}(k, \omega), \quad (25)$$

where $\gamma = \frac{e}{2m}$ is the gyromagnetic ratio, $\mu_B = \frac{e\hbar}{2m}$ is the Bohr magneton, and we have defined

$$L(k, \omega, \lambda_s) = \frac{\{2\Im\mathbf{m}(K_m)\lambda_s\}^2}{\{2\Im\mathbf{m}(K_m)\lambda_s\}^2 - 1}, \quad (26)$$

$$u_{\sigma}(k, \omega) = \epsilon_0 |E_{p\sigma}^m|^2. \quad (27)$$

On the other hand, the general solution of the corresponding homogeneous equation is

$$\delta\mu^0 = \sum_{\sigma} B_{\sigma} e^{-\sigma z / \lambda_s}. \quad (28)$$

When the two characteristic lengths are comparable, the factor $L(k, \omega, \lambda_s)$ becomes large and its sign can be flipped.

The coefficients, B_{σ} , are determined by the boundary condition that the derivative of the total spin accumulation (i.e., the diffusive spin current) vanishes at the two boundaries,

$$0 = \nabla \delta\mu|_{z=\pm d/2} = \nabla(\delta\mu^0 + \delta\mu^{\text{SP}})|_{z=\pm d/2}. \quad (29)$$

This yields simultaneous equations,

$$\begin{pmatrix} e^{-\frac{d}{2\lambda_s}} & -e^{+\frac{d}{2\lambda_s}} \\ e^{+\frac{d}{2\lambda_s}} & -e^{-\frac{d}{2\lambda_s}} \end{pmatrix} \begin{pmatrix} B_+ \\ B_- \end{pmatrix} = 2\Im\mathbf{m}(K_m)\lambda_s \begin{pmatrix} -e^{-\Im\mathbf{m}(K_m)d} & e^{+\Im\mathbf{m}(K_m)d} \\ -e^{+\Im\mathbf{m}(K_m)d} & e^{-\Im\mathbf{m}(K_m)d} \end{pmatrix} \begin{pmatrix} A_+ \\ A_- \end{pmatrix},$$

and then, we get

$$\begin{pmatrix} B_+ \\ B_- \end{pmatrix} = -\frac{\lambda_s}{d} \frac{X+Y}{\sinh(X-Y)} \begin{pmatrix} \sinh X & \sinh Y \\ \sinh Y & \sinh X \end{pmatrix} \begin{pmatrix} A_+ \\ A_- \end{pmatrix}, \quad (30)$$

where we have defined

$$X = \frac{d}{2\lambda_s} \{2\Im\mathbf{m}(K_m)\lambda_s + 1\},$$

$$Y = \frac{d}{2\lambda_s} \{2\Im\mathbf{m}(K_m)\lambda_s - 1\}.$$

Finally, we get the spin accumulation,

$$\delta\mu = \sum_{\sigma} A_{\sigma} e^{-2\sigma\Im\mathbf{m}(K_m)z} + B_{\sigma} e^{-\sigma z / \lambda_s}, \quad (31)$$

and the spin current driven by the spin accumulation,

$$\mathbf{j}_s = \frac{1}{\rho_0 e} \nabla \delta\mu \quad (32)$$

$$= -\frac{1}{\rho_0 e} \sum_{\sigma} \sigma \left(2\Im\mathbf{m}(K_m) A_{\sigma} e^{-2\sigma\Im\mathbf{m}(K_m)z} + \frac{1}{\lambda_s} B_{\sigma} e^{-\sigma z / \lambda_s} \right) \mathbf{u}_z. \quad (33)$$

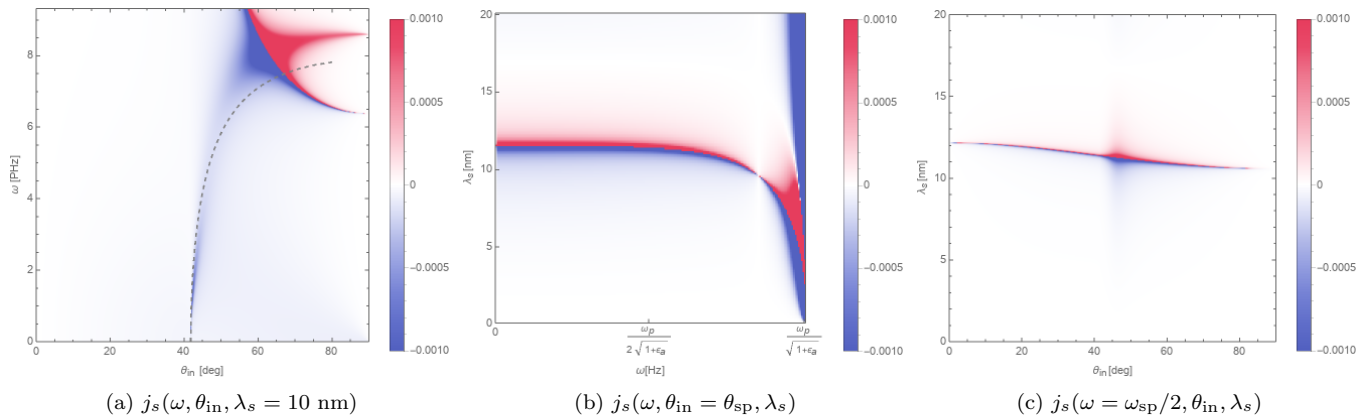


FIG. 6. Optically generated spin current j_s at $z = 0$ in the Kretschmann configuration. (a) colormap of j_s as a function of the incident frequency ω and the incident angle θ_{in} for a fixed spin diffusion length λ_s . The grey dashed line indicates the SP angle $\theta_{\text{sp}}(\omega)$. We can see that the peak of the spin current density is around the dashed curve, which implies the spin current is driven by the SP. The sign of the spin current is flipped, and the peak slightly deviate from the SP angle condition around the right top region, where the spontaneous diffusion dominates over the induced diffusion. (b) colormap of j_s as a function of the incident frequency ω and the spin diffusion length λ_s at the SP angle incidence $\theta_{\text{in}} = \theta_{\text{sp}}$. (c) colormap of j_s as a function of the incident angle θ_{in} and the spin diffusion length at a given frequency. To generate these plots, we set $\rho_0 = 12.8 \times 10^{-8}$ (the resistivity of gold), and other parameters are the same as the previous figures. Note that we set the upper and lower bounds of the plot ranges -10 mA/m^2 and 10 mA/m^2 so that the peaks can be seen clearly.

In FIG. 6, the spin current is shown as a function of the incident frequency ω , the incident angle θ_{in} , and the spin diffusion length of the metal λ_s . From FIG. 6a, we can see that the spin current peaks around the SP angle incidence. The peak deviates from the SP angle condition at high frequency region. This is because the decay length of the SP $\Im m(K_m)$ and the spin diffusion length λ_s are comparable in that region, and the spontaneous diffusion become comparable with the induced diffusion. Besides, we can observe the resonant response and the polarisation of the spin current is flipped there because the sign of the factor $L(k, \omega, \lambda_s)$ is flipped. We can also confirm the sign flip of the spin current both when it is plotted as a function of the incident frequency and the spin diffusion length and when plotted as a function of the incident angle and the spin diffusion length (see FIGs. 6b and 6c).

IV. CONCLUSION

To sum up, in this work, we have calculated a plasmonic system coupled to external laser drive where electron spin currents are generated.

In order to perform the analysis of electromagnetic field in the system, the scattering matrix formalism is utilised. Using the data provided by the field analysis, we

calculated magnetisation induced by plasma oscillation in the metal. Since the magnetisation inherits the frequency dependence, the incident angle dependence, and the spatial distribution from the plasmonic modes, it acts as inhomogeneous effective magnetic field which peaks at a condition where the surface plasmon mode is excited by the external drive and causes the Stern-Gerlach effect to generate electron spin current.

We have also solved spin diffusion equation to analyse the spin current in detail. There are two kind of diffusion process. One is the spontaneous diffusion which is characterised by the spin diffusion length of the metal. The other is induced by the plasmonic modes whose characteristic length is the penetration length of the electromagnetic field. When these two characteristic length match, the spin diffusion is resonantly enhanced and the polarisation of the spin current is flipped.

Our theoretical studies here are feasible for experimental demonstration and commit to further research on the interface between optics and spintronics.

ACKNOWLEDGMENTS

MM is partially Supported by the Priority Program of Chinese Academy of Sciences, Grant No. XDB28000000.

¹ J. Flipse, F. Dejene, D. Wagenaar, G. Bauer, J. B. Youssef, and B. Van Wees, Observation of the spin peltier effect for magnetic insulators, Physical review letters **113**, 027601

(2014).

² S. Daimon, R. Iguchi, T. Hioki, E. Saitoh, and K.-i. Uchida, Thermal imaging of spin peltier effect, Nature communi-

- cations **7**, 1 (2016).
- ³ G. Zolfagharkhani, A. Gaidarzhy, P. Degiovanni, S. Kettmann, P. Fulde, and P. Mohanty, Nanomechanical detection of itinerant electron spin flip, *Nature nanotechnology* **3**, 720 (2008).
 - ⁴ K. Harii, Y.-J. Seo, Y. Tsutsumi, H. Chudo, K. Oyanagi, M. Matsuo, Y. Shiomi, T. Ono, S. Maekawa, and E. Saitoh, Spin seebeck mechanical force, *Nature communications* **10**, 1 (2019).
 - ⁵ R. Vrijen, E. Yablonovitch, K. Wang, H. W. Jiang, A. Balandin, V. Roychowdhury, T. Mor, and D. DiVincenzo, Electron-spin-resonance transistors for quantum computing in silicon-germanium heterostructures, *Physical Review A* **62**, 012306 (2000).
 - ⁶ J. H. Wesenberg, A. Ardavan, G. A. D. Briggs, J. J. Morton, R. J. Schoelkopf, D. I. Schuster, and K. Mølmer, Quantum computing with an electron spin ensemble, *Physical review letters* **103**, 070502 (2009).
 - ⁷ R. Takahashi, M. Matsuo, M. Ono, K. Harii, H. Chudo, S. Okayasu, J. Ieda, S. Takahashi, S. Maekawa, and E. Saitoh, Spin hydrodynamic generation, *Nature Physics* **12**, 52 (2016).
 - ⁸ D. Kobayashi, T. Yoshikawa, M. Matsuo, R. Iguchi, S. Maekawa, E. Saitoh, and Y. Nozaki, Spin current generation using a surface acoustic wave generated via spin-rotation coupling, *Physical Review Letters* **119**, 077202 (2017).
 - ⁹ G. Okano, M. Matsuo, Y. Ohnuma, S. Maekawa, and Y. Nozaki, Nonreciprocal spin current generation in surface-oxidized copper films, *Physical Review Letters* **122**, 217701 (2019).
 - ¹⁰ K. Uchida, H. Adachi, D. Kikuchi, S. Ito, Z. Qiu, S. Maekawa, and E. Saitoh, Generation of spin currents by surface plasmon resonance, *Nature communications* **6**, 5910 (2015).
 - ¹¹ S. Ishii, K.-i. Uchida, T. D. Dao, Y. Wada, E. Saitoh, and T. Nagao, Wavelength-selective spin-current generator using infrared plasmonic metamaterials, *APL Photonics* **2**, 106103 (2017).
 - ¹² D. Oue and M. Matsuo, Electron spin transport driven by surface plasmon polaritons, *Physical Review B* **101**, 161404(R) (2020).
 - ¹³ D. Oue and M. Matsuo, Effects of surface plasmons on spin currents in a thin film system, *New Journal of Physics* **22**, 033040 (2020).
 - ¹⁴ M. Matsuo, Y. Ohnuma, T. Kato, and S. Maekawa, Spin current noise of the spin seebeck effect and spin pumping, *Physical review letters* **120**, 037201 (2018).
 - ¹⁵ T. Kato, Y. Ohnuma, M. Matsuo, J. Rech, T. Jonckheere, and T. Martin, Microscopic theory of spin transport at the interface between a superconductor and a ferromagnetic insulator, *Physical Review B* **99**, 144411 (2019).
 - ¹⁶ S. A. Maier, *Plasmonics: fundamentals and applications* (Springer Science & Business Media, Berlin, 2007).
 - ¹⁷ K. Y. Bliokh and F. Nori, Transverse spin of a surface polariton, *Physical Review A* **85**, 061801 (2012).
 - ¹⁸ K. Y. Bliokh, A. Y. Bekshaev, and F. Nori, Extraordinary momentum and spin in evanescent waves, *Nature Communications* **5**, 3300 (2014).
 - ¹⁹ A. Y. Bekshaev, K. Y. Bliokh, and F. Nori, Transverse spin and momentum in two-wave interference, *Physical Review X* **5**, 011039 (2015).
 - ²⁰ K. Y. Bliokh, D. Smirnova, and F. Nori, Quantum spin hall effect of light, *Science* **348**, 1448 (2015).
 - ²¹ T. Van Mechelen and Z. Jacob, Universal spin-momentum locking of evanescent waves, *Optica* **3**, 118 (2016).
 - ²² L. Fang and J. Wang, Intrinsic transverse spin angular momentum of fiber eigenmodes, *Physical Review A* **95**, 053827 (2017).
 - ²³ D. Oue, Dissipation effect on optical force and torque near interfaces, *Journal of Optics* **21**, 065601 (2019).
 - ²⁴ K. Y. Bliokh, A. Y. Bekshaev, and F. Nori, Optical momentum, spin, and angular momentum in dispersive media, *Physical Review Letters* **119**, 073901 (2017).
 - ²⁵ K. Y. Bliokh, A. Y. Bekshaev, and F. Nori, Optical momentum and angular momentum in complex media: from the abraham–minkowski debate to unusual properties of surface plasmon-polaritons, *New Journal of Physics* **19**, 123014 (2017).
 - ²⁶ M. Matsuo, J. Ieda, K. Harii, E. Saitoh, and S. Maekawa, Mechanical generation of spin current by spin-rotation coupling, *Physical Review B* **87**, 180402 (2013).
 - ²⁷ M. Matsuo, Y. Ohnuma, and S. Maekawa, Theory of spin hydrodynamic generation, *Physical Review B* **96**, 020401 (2017).